Research Article | Vol. 27, No. 2 | 21 Jan 2019 | OPTICS EXPRESS 1425
Optics EXPRESS

An opto-acousto-fluidic microscopic system with a high spatiotemporal resolution for microfluidic applications

FEI LIU,[1,2,5] TIAN JIN,[1,3,5] RUOPENG YAN,[4] TINGTING LI,[1] BIAO HU,[2] LEI YAO,[2] TIANYE HUANG,[4] CHAOLONG SONG,[4,6] AND LEI XI[1,*]

[1]*Department of Biomedical Engineering, Southern University of Science and Technology, Shenzhen, Guangdong, 518055, China*
[2]*School of Electronic Science and Engineering, University of Electronic Science and Technology of China, Chengdu, 610054, China*
[3]*School of Physics, University of Electronic Science and Technology of China, Chengdu, 610054, China*
[4]*School of Mechanical Engineering and Electronic Information, China University of Geosciences (Wuhan), Wuhan, 430074, China*
[5]*These authors contributed equally to this work*
[6]*songcl@cug.edu.cn*
[*]*xilei@sustc.edu.cn*

Abstract: In this work, we develop a new opto-acouto-fludic microsopic system, which employs a high-speed one-dimensional galvanometer scanner and an ultrafast pulse laser (600 kHz). The new system has achieved a high two-dimensional frame rate of up to 2500 Hz with a lateral resolution of 1.7 μm and an axial resolution of 36 μm at the imaging plane. To demonstrate the improved performance of the new system compared to our previous one, we carried out experiments to image the flowing droplets generated with T-junction and flow focusing configurations. We also successfully imaged dynamic migration of magneto particles subjected to non-uniform magnetic field in the microchannel. The results suggest that our new system has sufficient spatiotemporal resolutions to carry out studies for high throughput microfluidic applications.

1. Introduction

In the recent past, high throughput microfluidics have shown vast potentials in the fields of drug discovery [1], tissue engineering [2] and nanotechnology [3], as thousands of pharmacological, genetic or chemical samples can be processed and analyzed in a rapid manner on lab-on-chip platforms [4]. In such scenarios, high-speed detection schemes are required for real-time monitoring of micro-flows. Numerous methods have been proposed in recent years, such as surface-enhanced Raman scattering spectroscopy [5,6], electrical impedance-based sensing [7,8], laser-induced fluorescing [9–11], and dynamic light scattering [12]. Among these techniques, laser-induced fluorescing becomes the most popular one due to its high sensitivity and specificity [13,14]. Given the mechanism of fluorescing, sensitive optoelectronic sensors, such as photomultiplier tube and avalanche photodiode, are required to collect the signals for high-speed measurements [15–17], which unfortunately pin down the fluorescence-based techniques on single-point detection manner for high throughput microfluidic applications. The compromise between the temporal and spatial resolution cannot make the techniques adaptive to some occasions when both spatial and temporal information are important, such as the full-field measurement of concentration gradient and its variation rate in microchannels or distribution of cells within a flowing droplet. Additionally, labelling samples with fluorophores inevitably stain the analytes to some extent. Besides fluorescence, dynamic light scattering is only capable of providing statistical information of particles [12]. Optoacoustic imaging, a hybrid optical imaging modality with

#346932 https://doi.org/10.1364/OE.27.001425
Journal © 2019 Received 27 Sep 2018; revised 8 Dec 2018; accepted 9 Dec 2018; published 16 Jan 2019

Optics EXPRESS

rich optical contrast, high spatial resolution and deep penetration depth, is able to utilize both intrinsic and external contrasts for imaging/sensing of cells/particles [18,19]. In addition, it is free of depth scanning, making it capable of high-throughput three-dimensional imaging in microfluidic applications.

In our previous study, we demonstrated a microscopic technique based on optoacoustic imaging for label-free detection of flowing droplets and red blood cells in microchannels (referred to as G1 system) [20]. Owing to the limitation of a low-repetition-rate pulsed laser (50 kHz), the system can only work at a relatively low flow rate of micro-flows. As the microscopic system worked at reflection mode [21~23], the overlapping alignment of optics and acoustics did not offer the flexibility to optimize the imaging resolution. In this work, we re-align the optical and acoustic paths to make the imaging system work at a transmission mode, which can improve the lateral resolution to be 1.7 μm. A pulsed laser with an ultrahigh repetition rate of 600 kHz increases the frame rate up to 2500 Hz. To verify the performance of the new system, we carried out experiments to image the flowing droplets generated with T-junction and compared the results with those using our previous system. The comparison shows that the new system can capture the droplet images with a better spatiotemporal resolution and can work at a flow rate of 3 times higher than the previous one. To exploit the imaging capabilities of the new system, we also carried out experiments to successfully observe the magnetophoresis of particles in microchannels [24,25] and well resolve the smaller droplets including satellite droplets generated with flow-focusing devices [26].

2. Methods

2.1 System configuration

Figures 1(a) and 1(b) show the schematic of the transmission-mode opto-acousto-fluidic microscopic system and the volumetric layout of the imaging interface, respectively. Laser pulses with a duration of ~1.3 nanoseconds (ns) were emitted from a 532 nm pulsed laser (GLPM-10, IPG Photonics) at a repetition rate of up to 600 kHz. The laser beam profile was trimmed by an optical spatial filter (GCO-0112M, Daheng Optics), and focused using an objective, then coupled into a single-mode fiber via a space-to-fiber coupler (APFC-5T-FC, Beijing Zolix Intruments Co.). The output laser beam from the optical fiber was collimated via a fiber collimator (F220FC-532, Thorlabs Inc.), and steered by a fast 1-dimensional galvanometer scanner (GVS001, Thorlabs Inc.), driven by a multifunctional analog output device (PCI-6731, National Instrument). The laser beam was eventually focused by a 10 × objective (GCO-2112, Daheng Optics) to excite optoacoustic signals with an optical resolution. A spherically focused high-frequency transducer (V3332, Olympus) with an active area of 3 mm, a focal length of 12.7 mm, a center frequency of 50 MHz, and a bandwidth of 70% was used to collect optoacoustic signals. In our system, the dual foci of optical excitation and ultrasonic detection were configured confocally to maximize the systemic sensitivity [27]. The optoacoustic signals were amplified by a homemade pre-amplifier at ~64 dB, and digitized by a high-speed data acquisition card (ATS-9325, Alazar Inc.) at a sampling rate of 250 MS/s.

We initially measured the spatial resolution of the G2 system using a blade edge. Specifically, we obtained the distribution of lateral resolution in the focal plane by measuring the full width at half maxima (FWHM) of the line spread function (LSF) derived from the edge-spread function (ESF) of the imaged blade edge. To estimate the axial resolution, we did the Hilbert transform of a typical A-line and derived the FWHM of the signal envelop.

2.2 Chip preparation

We mainly used two different microfluidic devices, particularly with T-junction and flow focusing configurations, to demonstrate the high-speed imaging capability of the G2 system. The microfluidic chips were fabricated using standard soft-lithography with a channel height

Optics EXPRESS

of 100 μm. To minimize the acoustic attenuation of the optoacoustic signal, a PDMS membrane (thickness of 100 μm) was used for bonding and sealing the PDMS replica. Fluid samples were injected into the chips using syringe pumps (TYD02-01, Lead Fluid) via plastic tubes.

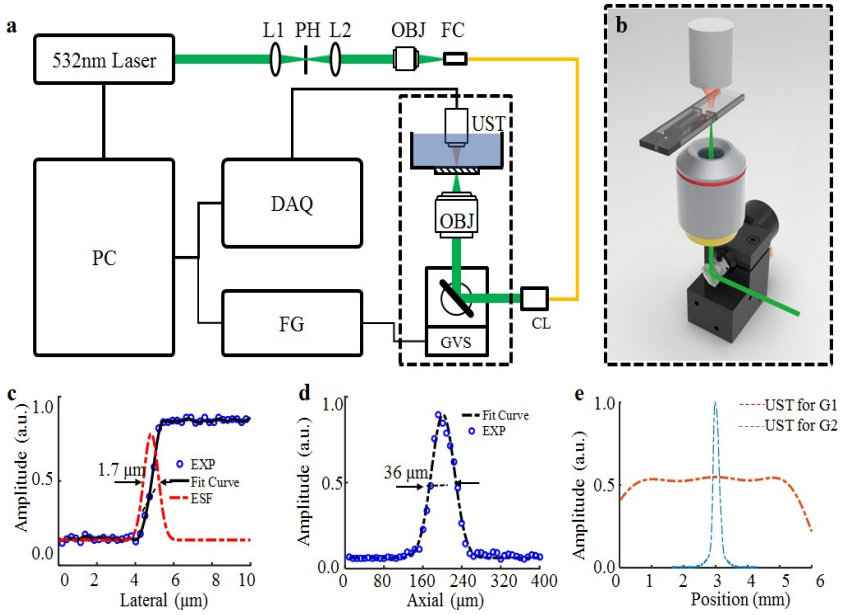

Fig. 1. (a) Schematic illustration of the opto-acousto-fluidic microscopic system. PC: personal computer, DAQ: data acquisition card, FG: function generator, L1: lens 1, L2: lens 2, PH: pinhole, OBJ: objective, UST: ultrasound transducer, FC: fiber coupler, CL: collimator lens, GVS: galvanometer scanner. (b) The layout of the imaging interface. (c) Evaluation of the lateral resolution. EXP: experiment, ESP: edge spread function. (d) Evaluation of the axial resolution. (e) Sensitivity comparison between cylindrically focused transducer (G1) and spherically focused high-frequency transducer (G2).

3. Results and discussion

3.1 System characterization

We evaluated the imaging resolution of the G2 system using a blade edge. The lateral resolution of the system is estimated to be 1.7 μm, as shown in Fig. 1(c). Figure 1(d) presents the measurement of the axial resolution (36 μm), which has been greatly improved compared to that of G1 system (60 μm). To investigate the detection sensitivity, we conducted experiments to compare the signals captured by the spherically focused ultrasound transducer (G2) and cylindrically focused ultrasound transducer (G1). It is shown that the amplitude can be greatly enhanced by two times when using the spherically focused transducer instead of the cylindrically focused transducer (Fig. 1(e)). Although the size of detection zone is shrinking to a diameter of 200 μm with the spherically focused transducer, it is still sufficient to cover the entire microchannel under inspection in our experiments. The details and comparisons of the system performance can be referred to Table 1.

In order to show the advantages of the G2 system visually, we conducted the droplets experiment by using a T junction. B-scans, which were acquired by scanning the laser spot across the microchannel, were captured at the downstream of the T-junction to image droplets. Specifically, ponceau 4R–water solution (with a strong EM absorbance spectrum around 510 nm) and mineral oil served as the dispersed and continuous phases, respectively.

Optics EXPRESS

Table 1. The comparison between the G1 andG2 systems

	G1	G2
Axial resolution (μm)	60	36
Lateral resolution (μm)	3.2	1.7
Scanning speed (Hz)	200	2500
Sensitivity (dB)	35	60

In terms of scanning speed, it is primarily limited by both the laser repetition rate and the maximum scanning speed of the galvanometer scanner. In G1 system, the minimum optical scanning angle is larger than 0.5 degree, leading to a maximum scanning speed of 250 Hz. In G2 system, due to the small scanning angle (<0.2°), the maximum scanning speed of the galvanometer is up to 2500 Hz. To demonstrate the highly improved imaging speed of the G2 system, we imaged the droplets with a B-scan rate of 500 Hz and 2500 Hz respectively under the same condition of droplets formation as shown in Figs. 2(a) and 2(b). The resolution in the flow direction is evaluated to be 23 μm in Fig. 2(a) and 5.8 μm in Fig. 2(b). Then we increased the total flow rate regularly while keeping the dispersed and continuous phases at the same flow rate ratio. We calculated the pixel number along the flow direction of each droplet at different flow rate and plotted them in Fig. 2(c). The results suggest that the scanning speed and the resolution in the flow direction of G2 system have been greatly improved compared to the G1 system.

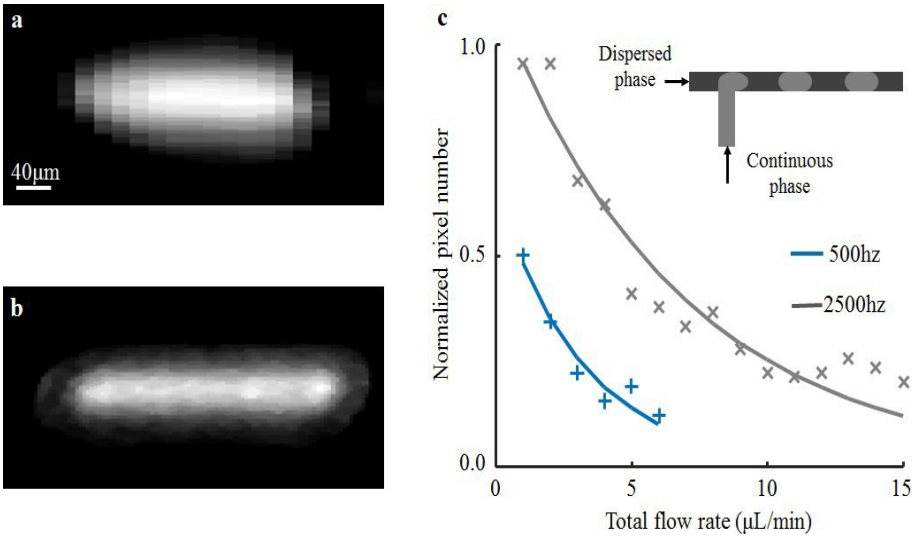

Fig. 2. Imaging droplet with G1 and G2 systems. (a) Droplet imaged by G1 system with lateral resolution of 3.2 μm, axial resolution of 60 μm, and resolution in flow direction of 23 μm. The total flow rate is 7 μl/min, and the flow rate ratio is 1. (b) Droplet imaged by G2 system with lateral resolution of 1.7 μm, axial resolution of 36 μm, and resolution in flow direction of 5.8 μm. The total flow rate is 7 μl/min, and the flow rate ratio is 1. (c) Comparison of normalized pixel number of the imaged droplets retrieved at different total flow rates between the B-scan rates of 500 Hz and 2500 Hz. The inset illustrates the droplets formed at a T-junction. (a) and (b) share the same scale bar.

3.2 Microspheres experiments

Magnetic micro-particles have been extensively explored in magnetic resonance imaging, hyperthermia, targeted delivery of therapeutics and separation of cells. The G2 system with improved temporal and spatial resolutions enable the detection of the flowing particles with decent resolution and sensitivity. We use the affimag SLC Magnetic particles (Tianjin BaseLine Chrom Tech Research Centre) with an average diameter of 2 μm. The volume fraction of the magnetic particles is 0.5%. We diluted the magnetic particles solute of 1 μL into 2 mL water, and set the flow rate at 1 μL/min. Firstly, we imaged the particles without

Optics EXPRESS

applying non-uniform magnetic field. The particles were distributed randomly in the microchannel as shown in Fig. 3(a). Then we allocated a cube magnet with a length of 5 mm at two sides of the channel separately to exert magnetic forces on the flowing particles. Under the magnetic and flow drag forces, particles started to migrate and aggregate at the channel walls as shown in Figs. 3(b) and 3(c). Figures 3(d)-3(f) show the signal profile along the transverse direction of the micro- channel. The upper right corner of each figure is placed by magnet. The magnet is 2 mm at the horizontal direction close to the channel.

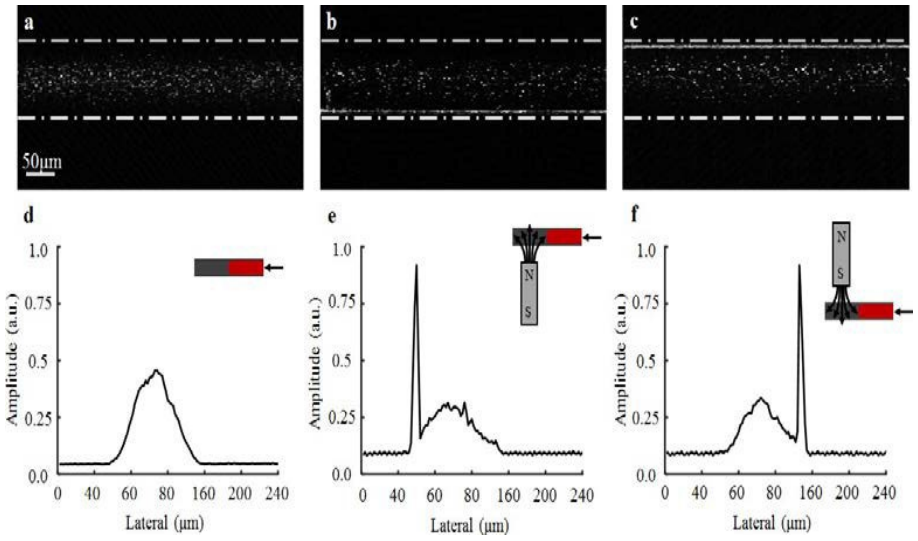

Fig. 3. Imaging and monitoring of magneto-particles migrating in microchannels. (a) Imaging magneto-particles without applying magnetic field. (b) Imaging magneto-particles with magnet allocated at the lower side of microchannel (c) Imaging micro- particles with magnet at upper side of microchannel. (d) ~(f) The signal profiles along the transverse direction of the microchannel corresponding to (a) ~(c), respectively. (a), (b) and (c) share the same scale bar.

3.3 Imaging droplets generated with flow focusing configuration

A number of applications have been found with droplets produced using flow-focusing configuration, such as drug discovery [28] and molecular genetics [29], particularly when the droplet size and the spatial distribution can be prescribed on a micro or nanoscale. Droplet production rate in flow focusing devices can be up to tens of kHz [30] and minimum droplet size can be manipulated to several hundred nanometers [31]. Although many methods have been demonstrated for effective control of droplet size, including using hydrodynamic [32], thermal [33] and electrical actuations [34], yet the only way for in-line monitoring of droplet formation dynamics has been with high-speed photography [35]. The methodology generally requires using a high-speed camera and produces overwhelming data per unit time, which could impose a challenge on instantaneous data processing and subsequent feedback-based control for droplet-on-demand (DoD) applications [36]. Herein, we demonstrate to monitor the dynamics of droplet formation using our high-speed opto-acousto-fluidic microscopic system. As the collected opto-acoustic signal is analog, it is facile to process the data possibly for either real-time displaying or possibly serving as feedback signal.

In the experiment, flow-focusing configuration was used to produce droplets at different formation regimes. In particular, the channel height is 100 μm. The width of center channel containing aqueous phase and the outer channel containing oil phase (W1) are both 200 μm. The width of the orifice (W2) is 50 μm, the total width (W3) of the channel is 500 μm. In the experiment, the flow rate of aqueous phase was fixed at 0.6 μl/min, and the flow rate ratio was varied by increasing the flow rate of mineral oil. As shown in Fig. 4(a), when the mineral oil flow rate was set to be 1.5 μl/min, droplets of various sizes can be generated. The

Optics EXPRESS

diameters of these droplets ranged from 21 to 60 μm. The non-uniformity of droplet sizes can be attributed to the occasional coalescence of droplets flowing at low velocities. When mineral oil flow rate was increased to be 6 μl/min, droplets with relatively uniform size (diameter of 100 μm) was generated and observed, as shown in Fig. 4(b). Satellite droplets, which break up at the orifice, can also be regularly produced in this droplet formation regime. When the flow rate of the mineral oil was increased to be 15 μl/min, droplets with size much smaller than that of orifice was generated and flowing in a row to downstream (Fig. 4(c)). The dynamics of droplet formation recorded by our opto-acousto-fluidic microscopic system is similar and consistent with previous studies [37,38].

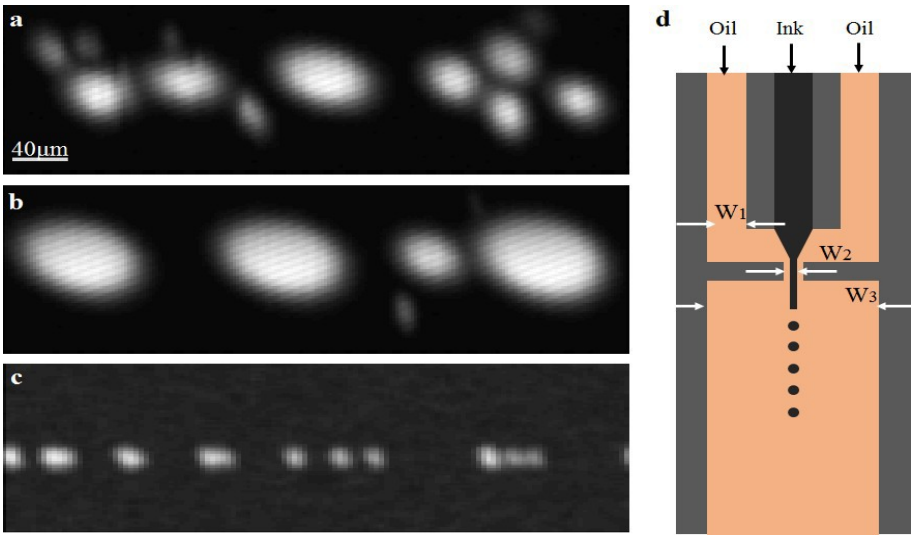

Fig. 4. Imaging of droplets generated with flow-focusing configuration. (a) Imaged droplet under flow rates of Q_i = 0.6 μl/min and Q_0 = 1.5 μl/min. (b) Imaged droplet under flow rates of Q_i = 0.6 μl/min and Q_0 = 6 μl/min. (c) Imaged droplet under flow rates of Q_i = 0.6 μl/min and Q_0 = 15 μl/min. (d) The schematic of flow focusing device. (a), (b) and (c) share the same scale bar.

4. Conclusion

In summary, we report the design and evaluation of a new opto-acousto-fluidic microscopic system. By updating the objective and the laser, this new designed system can provide a better performance with a lateral resolution of 1.7 μm, an axial resolution of 36 μm and a B-scan rate up to 2500 Hz. Experiments are carried out to image the flowing droplets generated with T-junction microchannel and the results are compared with that of using our previous system. The comparison shows that the new system can capture the droplet images with much higher resolutions and can work at a flow rate of 3 times higher than the previous one. To exploit the capabilities of the new system, we also carry out experiments to successfully observe the magnetophoresis of particles in microchannels and well resolve the smaller droplets including satellite droplets generated with flow-focusing devices. Comparing the excellent performance of the upgraded system and mainly cost in laser, the investment is obviously worthwhile. With the highly improved spatiotemporal resolution, we envision that the new opto-acousto-fluidic microscopic system can be used for high throughput microfluidic applications.

Funding

National Natural Science Foundation of China (61775028, 81571722, 61804138, 61528401); the startup grant from Southern University of Science and Technology; Hubei Provincial Natural Science Foundation of China (2017CFB193).

Optics EXPRESS

References

1. P. S. Dittrich and A. Manz, "Lab-on-a-chip: microfluidics in drug discovery," Nat. Rev. Drug Discov. **5**(3), 210–218 (2006).
2. A. Khademhosseini, R. Langer, J. Borenstein, and J. P. Vacanti, "Microscale technologies for tissue engineering and biology," Proc. Natl. Acad. Sci. U.S.A. **103**(8), 2480–2487 (2006).
3. W. Li, L. Zhang, X. Ge, B. Xu, W. Zhang, L. Qu, C. H. Choi, J. Xu, A. Zhang, H. Lee, and D. A. Weitz, "Microfluidic fabrication of microparticles for biomedical applications," Chem. Soc. Rev. **47**(15), 5646–5683 (2018).
4. G. Du, Q. Fang, and J. M. J. den Toonder, "Microfluidics for cell-based high throughput screening platforms - A review," Anal. Chim. Acta **903**, 36–50 (2016).
5. K. Kant and S. Abalde-Cela, "Surface-Enhanced Raman Scattering Spectroscopy and Microfluidics: Towards Ultrasensitive Label-Free Sensing," Biosensors (Basel) **8**(3), 62 (2018).
6. Y. Zhang, S. Zhao, J. Zheng, and L. He, "Surface-enhanced Raman spectroscopy (SERS) combined techniques for high-performance detection and characterization," Trac-Trend. Anal. Chem. **90**, 1–13 (2017).
7. R. Reale, A. D. Ninno, L. Businaro, P. Bisegna, and F. Caselli, "Electrical measurement of cross-sectional position of particles flowing through a microchannel," Microfluid. Nanofluidics **22**(4), 41 (2018).
8. Y. Zhao, K. Wang, D. Chen, B. Fan, Y. Xu, Y. Ye, J. Wang, J. Chen, and C. Huang, "Development of microfluidic impedance cytometry enabling the quantification of specific membrane capacitance and cytoplasm conductivity from 100,000 single cells," Biosens. Bioelectron. **111**, 138–143 (2018).
9. P. S. Dittrich and A. Manz, "Single-molecule fluorescence detection in microfluidic channels--the Holy Grail in muTAS?" Anal. Bioanal. Chem. **382**(8), 1771–1782 (2005).
10. Y. Zhu and Q. Fang, "Analytical detection techniques for droplet microfluidics--a review," Anal. Chim. Acta **787**(13), 24–35 (2013).
11. M. Ugawa, C. Lei, T. Nozawa, T. Ideguchi, D. Di Carlo, S. Ota, Y. Ozeki, and K. Goda, "High-throughput optofluidic particle profiling with morphological and chemical specificity," Opt. Lett. **40**(20), 4803–4806 (2015).
12. E. Gulari, E. Gulari, Y. Tsunashuma, and B. Chu, "Photon correlation spectroscopy of particle distributions," J. Chem. Phys. **70**(8), 3965–3972 (1979).
13. S. Cesaro-Tadic, G. Dernick, D. Juncker, G. Buurman, H. Kropshofer, B. Michel, C. Fattinger, and E. Delamarche, "High-sensitivity miniaturized immunoassays for tumor necrosis factor α using microfluidic systems," Lab Chip **4**(6), 563–569 (2004).
14. C. Song and S. Tan, "A Perspective on the Rise of Optofluidics and the Future," Micromachines (Basel) **8**(5), 152 (2017).
15. D. Pekin, Y. Skhiri, J. C. Baret, D. Le Corre, L. Mazutis, C. B. Salem, F. Millot, A. El Harrak, J. B. Hutchison, J. W. Larson, D. R. Link, P. Laurent-Puig, A. D. Griffiths, and V. Taly, "Quantitative and sensitive detection of rare mutations using droplet-based microfluidics," Lab Chip **11**(13), 2156–2166 (2011).
16. L. Mazutis, J. Gilbert, W. L. Ung, D. A. Weitz, A. D. Griffiths, and J. A. Heyman, "Single-cell analysis and sorting using droplet-based microfluidics," Nat. Protoc. **8**(5), 870–891 (2013).
17. M. Srisa-Art, A. J. deMello, and J. B. Edel, "High-Throughput DNA Assays Using Picoliter Reactor Volumes," Biophys. J. **96**(3), 544 (2009).
18. E. I. Galanzha, E. V. Shashkov, P. M. Spring, J. Y. Suen, and V. P. Zharov, "In vivo, noninvasive, label-free detection and eradication of circulating metastatic melanoma cells using two-color photoacoustic flow cytometry with a diode laser," Cancer Res. **69**(20), 7926–7934 (2009).
19. E. I. Galanzha and V. P. Zharov, "Photoacoustic flow cytometry," Methods **57**(3), 280–296 (2012).
20. C. Song, T. Jin, R. Yan, W. Qi, T. Huang, H. Ding, S. H. Tan, N. T. Nguyen, and L. Xi, "Opto-acousto-fluidic microscopy for three-dimensional label-free detection of droplets and cells in microchannels," Lab Chip **18**(9), 1292–1297 (2018).
21. T. Jin, H. Guo, H. Jiang, B. Ke, and L. Xi, "Portable optical resolution photoacoustic microscopy (pORPAM) for human oral imaging," Opt. Lett. **42**(21), 4434–4437 (2017).
22. W. Qin, T. Jin, H. Guo, and L. Xi, "Large-field-of-view optical resolution photoacoustic microscopy," Opt. Express **26**(4), 4271–4278 (2018).
23. T. Jin, H. Guo, L. Yao, H. Xie, H. Jiang, and L. Xi, "Portable optical-resolution photoacoustic microscopy for volumetric imaging of multiscale organisms," J. Biophotonics **11**(4), e201700250 (2018).
24. N. Pamme and C. Wilhelm, "Continuous sorting of magnetic cells via on-chip free-flow magnetophoresis," Lab Chip **6**(8), 974–980 (2006).
25. J. Lim, C. Lanni, E. R. Evarts, F. Lanni, R. D. Tilton, and S. A. Majetich, "Magnetophoresis of nanoparticles," ACS Nano **5**(1), 217–226 (2011).
26. Y. C. Tan, J. S. Fisher, A. I. Lee, V. Cristini, and A. P. Lee, "Design of microfluidic channel geometries for the control of droplet volume, chemical concentration, and sorting," Lab Chip **4**(4), 292–298 (2004).
27. Q. Chen, T. Jin, W. Qi, X. Mo, and L. Xi, "Label-free photoacoustic imaging of the cardio-cerebrovascular development in the embryonic zebrafish," Biomed. Opt. Express **8**(4), 2359–2367 (2017).
28. Y. C. Tan, V. Cristini, and A. P. Lee, "Monodispersed microfluidic droplet generation by shear focusing microfluidic device," Sensor. Actuat. B. **114**(1), 350–356 (2006).

Optics EXPRESS

29. M. A. Burns, C. H. Mastrangelo, T. S. Sammarco, F. P. Man, J. R. Webster, B. N. Johnsons, B. Foerster, D. Jones, Y. Fields, A. R. Kaiser, and D. T. Burke, "Microfabricated structures for integrated DNA analysis," Proc. Natl. Acad. Sci. U.S.A. **93**(11), 5556–5561 (1996).
30. L. Yobas, S. Martens, W. L. Ong, and N. Ranganathan, "High-performance flow-focusing geometry for spontaneous generation of monodispersed droplets," Lab Chip **6**(8), 1073–1079 (2006).
31. A. M. G. Calvo, R. G. Prieto, P. R. Chueca, M. A. Herrada, and M. F. Mosquera, "Focusing capillary jets close to the continuum limit," Nat. Phys. **3**(10), 737–742 (2007).
32. V. van Steijn, C. R. Kleijn, and M. T. Kreutzer, "Predictive model for the size of bubbles and droplets created in microfluidic T-junctions," Lab Chip **10**(19), 2513–2518 (2010).
33. T. H. Ting, Y. F. Yap, N. T. Nguyen, T. N. Wong, J. C. K. Chai, and L. Yobas, "Thermally mediated breakup of drops in microchannels," Appl. Phys. Lett. **89**(23), 234101 (2006).
34. H. Ren, R. B. Fair, and M. G. Pollack, "Automated on-chip droplet dispensing with volume control by electro-wetting actuation and capacitance metering," Sensor. Actuat. B. **98**(2), 319–327 (2004).
35. S. L. Anna, N. Bontoux, and H. A. Stone, "Formation of dispersions using 'flow focusing' in microchannels," Appl. Phys. Lett. **82**(3), 364–366 (2003).
36. C. Girabawe and S. Fraden, "An image-driven drop-on-demand system," Sensor. Actuat. B-chem. **238**, 532–539 (2017).
37. W. Lee, L. M. Walker, and S. L. Anna, "Role of geometry and fluid properties in droplet and thread formation processes in planar flow focusing," Phys. Fluids **21**(3), 032103 (2009).
38. S. L. Anna and H. C. Mayer, "Microscale tipstreaming in a microfluidic flow focusing device," Phys. Fluids **18**(12), 121512 (2006).